Optical properties of black silicon structures ALD-coated with Al$_2$O$_3$

David Schmelz[1] **, Kristin Gerold**[1,2]**, Thomas Käsebier**[1]**, Natali Sergeev**[1]**, Adriana Szeghalmi**[1,2] **and Uwe D Zeitner**[1,2]

[1] Institute of Applied Physics, Abbe Center of Photonics, Friedrich Schiller University Jena, Germany
[2] Fraunhofer Institute for Applied Optics and Precision Engineering IOF, Jena, Germany

E-mail: david.schmelz@uni-jena.de

CrossMark

Abstract

Atomic layer deposited (ALD) Al$_2$O$_3$ coatings were applied on black silicon (b-Si) structures. The coated nanostructures were investigated regarding their reflective and transmissive behaviour. For a systematic study of the influence of the Al$_2$O$_3$ coating, ALD coatings with a varying layer thickness were deposited on three b-Si structures with different morphologies. With a scanning electron microscope the morphological evolution of the coating process on the structures was examined. The optical characteristics of the different structures were investigated by spectral transmission and reflection measurements. The usability of the structures for highly efficient absorbers and antireflection (AR) functionalities in the different spectral regions is discussed.

Keywords: black silicon, Al$_2$O$_3$, atomic layer deposition, antireflective structures, light trapping

(Some figures may appear in colour only in the online journal)

1. Introduction

Black silicon (b-Si) nanostructures are well known for their capabilities as antireflection (AR) and light-trapping structures. As such, they have a wide range of applications, for example, in solar cells [1–4], absorbers [5–7], IR optics [8], photoelectrochemical (PEC) hydrogenation [9], photothermic conversion [10] or Si-platform photodetectors [11–14]. Especially in the application on solar cells, they show a significantly improved performance compared to commonly used micro-scale random pyramids [1, 15, 16]. For optoelectronic devices, like solar cells, it is necessary to apply a thin conformal oxide coating for the passivation of the large surface area exposed by the b-Si structure. This prevents strong surface recombination effects and increases the carrier lifetimes significantly [17–19]. For passivation purposes, it is state of the art to apply thin Al$_2$O$_3$ coatings by atomic layer deposition (ALD) due to the achievable high conformity and low defect density [17–20]. Typical Al$_2$O$_3$ passivation coatings have a thickness of 10–30 nm [1, 13, 16]. By using a thin ALD coating,

the AR effect of the b-Si structures can be even further improved [1, 5]. In addition, Al$_2$O$_3$ coatings can serve as protection layers against diffusion and (chemical and mechanical) degradation in harsh environments [21, 22].

Even though the ascertained experimental results achieved with Al$_2$O$_3$-coated b-Si are promising, the main drawback of these structures is their mechanical instability. By an increase of the layer thickness, we expect an improvement of the mechanical stability of the coated b-Si structures and thus an extension of their potential application. In this regard, Otto [20] also noted an increase in carrier lifetimes for thicker Al$_2$O$_3$ coatings.

While the influence of the Al$_2$O$_3$ coatings on the electrical properties of b-Si structures is well studied, there is little information on the influence of the Al$_2$O$_3$ coatings on the optical properties of b-Si structures. In particular, no systematic studies on the dependence on the layer thickness could be found. Since we expect a significant increase in stability for higher layer thicknesses, we investigate their influence on reflection and transmission. Due to its bandgap at 1.12 eV, Si is absorptive up to about 1.1 μm wavelength. While reflection is of greater relevance for absorption and detection purposes, specular transmission is crucial for AR applications at longer wavelengths.
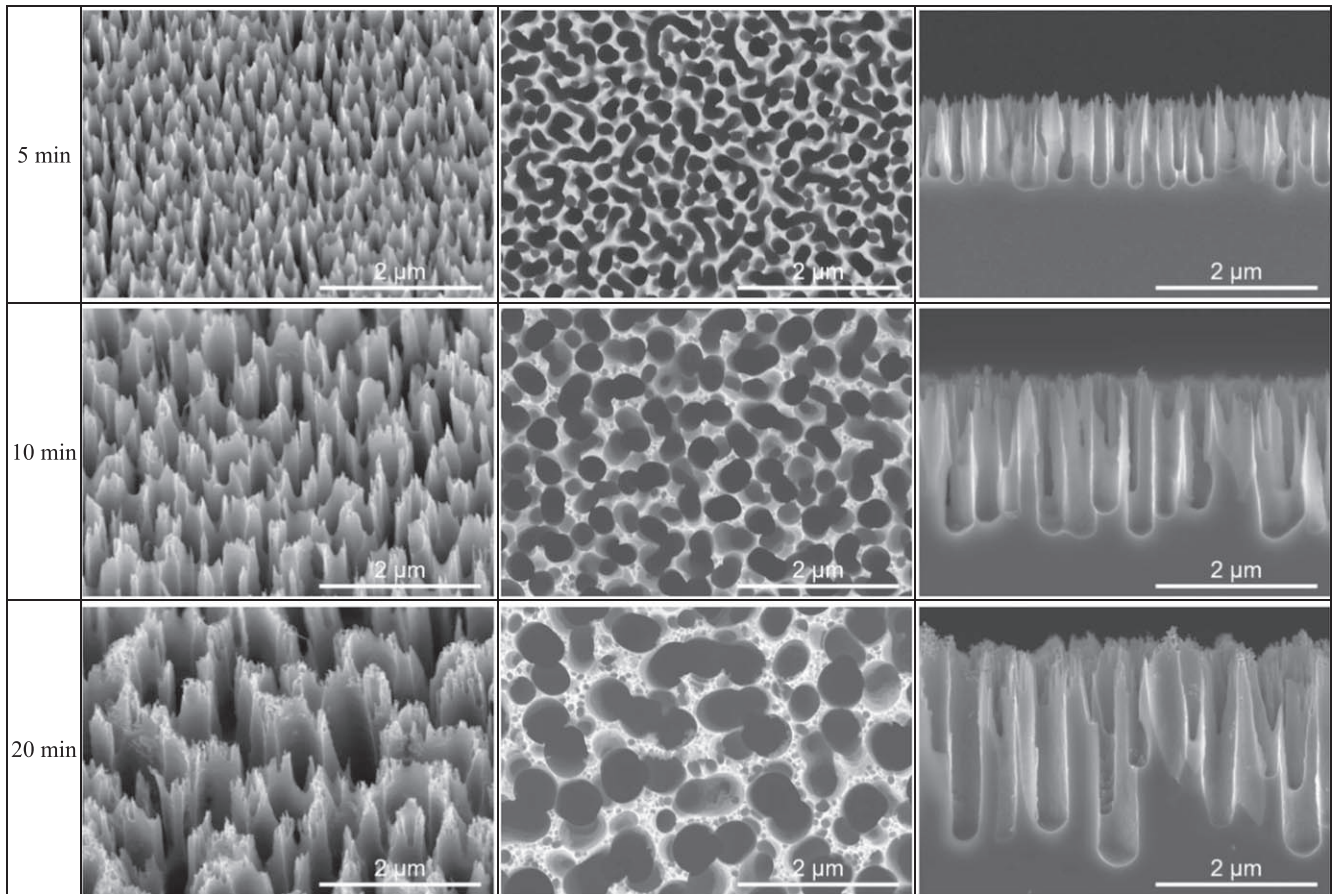
Figure 1. SEM images of b-Si structures with different etching times at 30° oblique view, top view and cross-sectional view.

2. Experimental details

2.1. Fabrication

The b-Si nanostructures were fabricated on only one side of 100 mm Si wafers (double-side polished (dsp), CZ, 5–10 Ω^*cm, p-doped) by an inductively coupled plasma reactive ion etching process (ICP-RIE) with SF_6 as etchant gas. The addition of O_2 stimulates the generation of silicon oxyfluorides which protects the Si from chemical etching. Because of their instability to heat and ion bombardment, they primarily cause passivation of the sidewalls, keeping them smooth and promoting etching in a vertical preferential direction. The addition of O_2 is thus essential to the self-masking process that allows the formation of b-Si [23, 24]. The etching process is carried out at low temperatures (-40 °C to -30 °C) and is based on a fabrication process that has been established over the past years [24]. Three different samples varying in etching times of 5, 10 and 20 min were processed at a pressure of 2 Pa, a SF_6 and O_2 flow of 60 sccm each, a 13.56 MHz RF power of 10 W and a moderate ICP power of 750 W at a starting temperature of -40 °C increasing slightly over etching time.

After structuring, the wafers were diced into 25×25 mm^2 chips. Subsequently, conformal Al_2O_3 coatings with various thicknesses were deposited using a plasma-enhanced ALD (PEALD) process (OpAL, Oxford Instruments). For the deposition process, trimethylaluminum (TMA) was used as metal-organic precursor and O_2 plasma as oxygen source. Depositions were carried out at temperatures of 100 °C. The Al_2O_3 layer thickness was determined on unstructured Si witness samples by spectroscopic ellipsometry (M2000, J.A. Woollam) and found to be 30 nm, 60 nm, 100 nm, 200 nm, 400 nm and 600 nm on the polished surfaces. It should be noted, however, that the significantly increased surface area of the nanostructures results in substantially higher material deposition in total.

2.2. Characterisation

After preparation, the samples were characterised in a Hitachi 4800 scanning electron microscope (SEM) regarding their structural morphology. Subsequently, the samples were optically analysed in two different measurement setups. In a Lambda 950 spectrometer (Perkin Elmer) with an included 150 mm integration sphere setup the hemispherical reflectance between 300 and 2000 nm wavelength was measured. The standard angle of incidence for that reflection setup is 8°. In addition, the specular transmission over a spectral range of 1000 to 2000 nm was measured with an angle of incidence of 0°. For wavelengths in the infrared range, transmission measurements were done in an Excalibur Series 3100 FTIR spectrometer (Varian, now Agilent Technologies) for wavelengths of 1.7–25 μm.
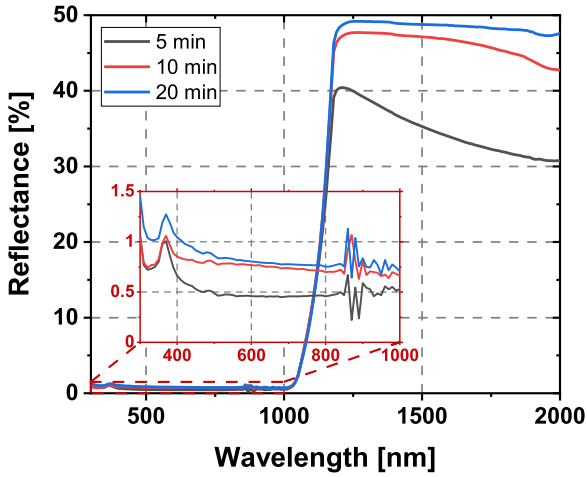
Figure 2. Hemispherical reflectance of uncoated b-Si structures at wavelengths from 300 to 2000 nm.
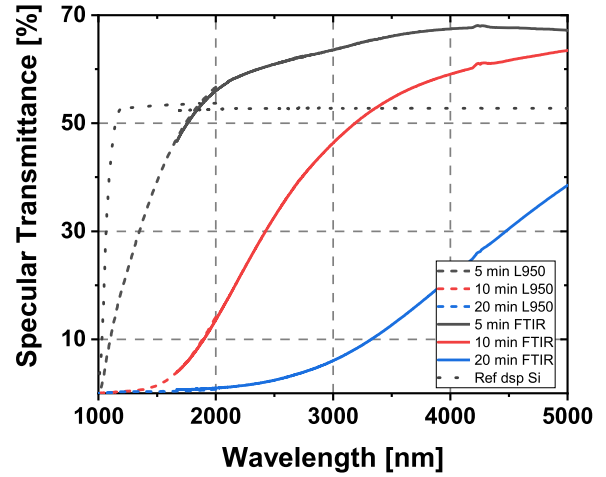

Figure 4. Specular transmittance of uncoated b-Si samples measured by Lambda 950 spectrometer and FTIR spectrometer.
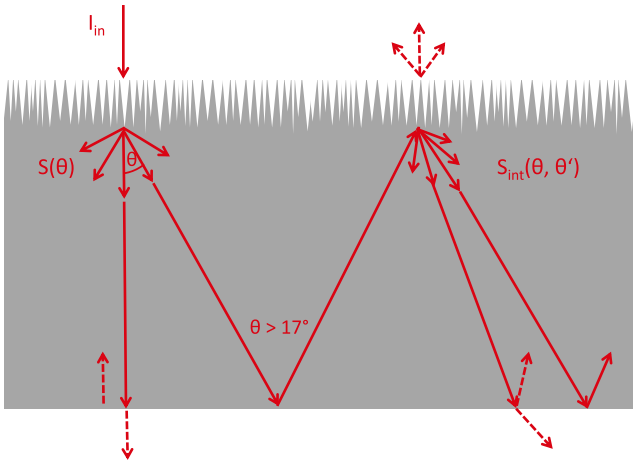

Figure 3. Principle schematic of the light trapping effect.

Figure 5. Specular transmittance of uncoated b-Si samples measured by FTIR spectrometer over a spectrum from 1.7 to 25 μm.

Table 1. Structural parameters of b-Si structures.

Etching time	5 min	10 min	20 min
Depth [μm]	1.2	2.1	3.3
Correlation length [nm]	159	258	456

3. Results and discussion

3.1. Uncoated black silicon structures

The b-Si morphology can be described by two main structural parameters: the structure height and the lateral correlation length. The former is estimated by a SEM cross-section inspection. The latter is a gauge for the lateral dimension of the nanostructures and related to the mean etch pore diameter. It is determined from the autocorrelation function of a top view SEM image. For this, the two-dimensional autocorrelation function is calculated from the image and subsequently accumulated and averaged over a radial line at each polar angle. As described by Steglich *et al* [24], structure
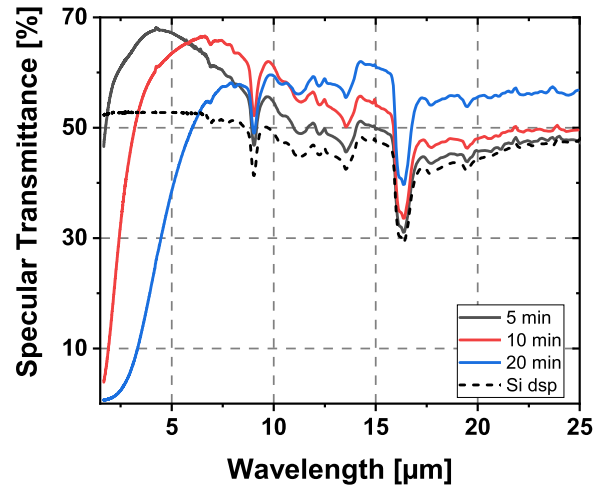
depth and correlation length are related to each other. With a longer etching time, there is an increase in both parameters [24]. Figure 1 shows each of the uncoated structures at three different views: a tilt angle of 30° (left), a top view (centre) and a cross-sectional view (right). Table 1 lists the determined values for structure height and correlation length for the three structures presented.

Figure 2 depicts the hemispherical reflectance of the uncoated structures at wavelengths from 300 to 2000 nm. For shorter wavelengths, displayed enlarged in figure 2, the hemispherical reflectance of the structures is in the range of 1% and shows approximately a similar behaviour for the three different structures. Among the structures, the 5 min etched sample has the lowest reflectance values (∼0.5%). At wavelengths between 860 and 920 nm, there are stronger fluctuations in the measured values, which are characteristic for the used Lambda 950 spectrometer and are caused by a switch in the measuring photodetectors. However, these are not of high relevance for the aspects to investigate.
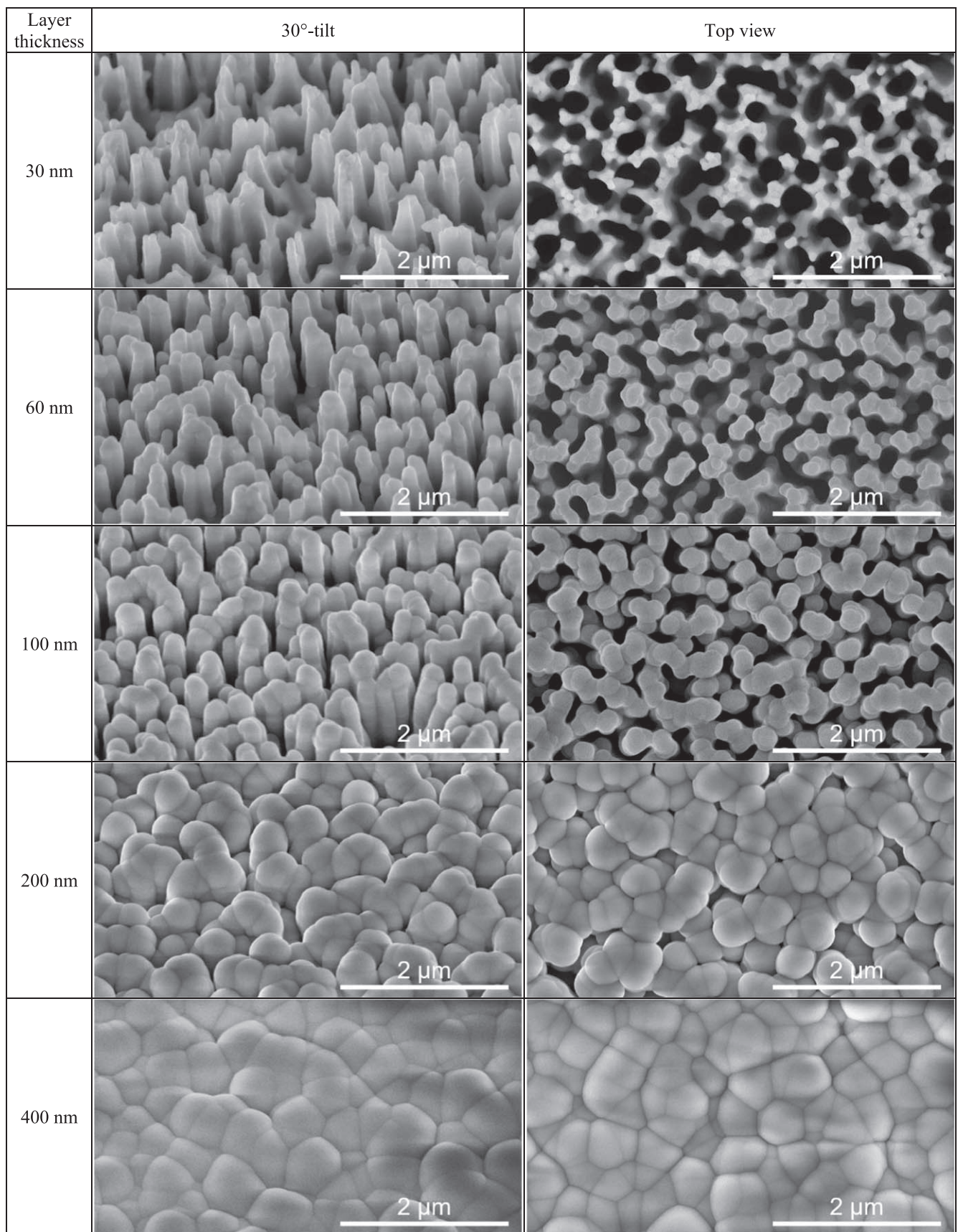
Layer thickness	30°-tilt	Top view
30 nm		
60 nm		
100 nm		
200 nm		
400 nm		

Figure 6. b-Si structures, 10 min etched, deposited with Al_2O_3 with increasing layer thickness.

From a wavelength of 1050 nm, the reflectance rises strikingly as the Si substrates lose their absorptive properties in this range. The reflection then derives from the polished backside of the substrates. While the Fresnel's reflectance at the interface between Si ($n \sim 3.49$) and air at normal incidence is about 30%, considerably higher reflectance values were observed here, which cannot be explained by an increasing reflectance of the b-Si surface. Instead, the higher reflectance is caused by a transmissive scattering effect into the Si substrate when passing the b-Si structure. For higher scattering angles, the internal reflectance increases and ends up in total reflection for angles $>17°$ [11, 25, 26]. Thus, portions of light may propagate several cycles through the substrate before leaving it, either transmitted or reflected. The resulting light trapping effect (with the difference that light is not absorbed) is illustrated graphically in figure 3.

The multiple reflection of the scattered light leads to a randomization of the propagating light within the Si substrate. The randomized light thus leaves both surfaces of the substrate in a more equalized ratio. This results in an upward shift in the total amount of back-reflected light. This effect becomes particularly clear when considering the reflectance of the 5 min etched sample in figure 2. Comprehensible for stochastic nanostructures with a certain distribution of lateral dimensions, the amount of scattered light increases for shorter wavelengths due to the greater amount of structures that are larger than the wavelength. For longer wavelengths instead, the scattering effect diminishes and turns into a sub-wavelength-based AR effect, eventually approximating the Fresnel reflections of front ($<1\%$) and back side ($\sim30\%$).

For the two other b-Si samples with larger structures (10 min, 20 min) the amount of scattered light is even higher. Hence, the light trapping effect is more prominent, which results in a higher reflectance. In the right margin of figure 2, the graph of the 10 min etched sample already indicates a similar approximating decay to the Fresnel reflection when moving further towards longer wavelengths in the IR range. This corresponds to the measurements of the specular transmission. Figure 4 combines the measurements of the specular transmission in the Lambda 950 spectrometer and the FTIR spectrometer. The 5 min etched sample shows a strong increase in the specular transmittance starting already at 1000 nm wavelength and reaching its maximum at 4270 nm. For the other two samples instead, transmissive scattering dominates in the shortwave infrared (SWIR, $1–3$ μm wavelength) due to the larger lateral dimensions. Accordingly, the specular transmission first starts to increase at longer wavelengths.

For AR applications, the transmissive behaviour of b-Si structures in the infrared regime is of importance. Figure 5 shows the specular transmission measured by the FTIR spectrometer from 1.7 to 25 μm wavelength. Hereby, former results by Steglich *et al* [8] could be confirmed. The measurements show that b-Si structures act as AR structures for infrared Si optics. Therefore, the etching process, e.g. the etching time, must be adapted to the spectral range of the application. Especially for wavelengths in the midwave infrared (MWIR, $3–5$ μm wavelength), the AR structures come close to the ideal transmission value of 70% for one-
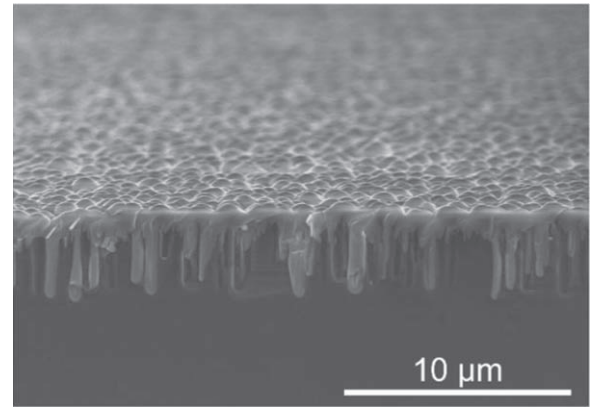

Figure 7. Cross-sectional view (10°) of 20 min etched sample coated with 600 nm Al_2O_3.

side structured Si samples and thus provide a conceivable alternative to AR coatings on Si optics. The challenge, however, is the fabrication of structures with an AR effect over a broader spectral range. Therefore, structures with higher aspect ratios are favourable.

3.2. Influence of Al_2O_3 coatings

Proceeding from the values of the uncoated b-Si structures, in the following the influence of the Al_2O_3 coatings on the structures and their optical behaviour is examined. Figure 6 illustrates the evolution of the structural morphology with increase in Al_2O_3 layer thickness. With increasing layer thickness, the initially sharp edges become rounder until the structures are completely filled with Al_2O_3 (see figure 7). Based on the images shown, an increasing mechanical stabilisation with increasing layer thickness is presumed.

Figure 8 shows the hemispherical reflectance of the structures coated with different thicknesses of Al_2O_3 at wavelengths from 300 to 1000 nm. All three investigated b-Si structures show comparable reflective behaviour in the VIS and NIR spectral range. Up to thicknesses of 100 nm, the reflectance is in a comparable range to that of the uncoated structures. Partially, the reflectance is also below. For 30 nm Al_2O_3, the hemispherical reflectance is improved over the entire spectral range. It should be emphasised that for all layer thicknesses investigated, the reflectance is still below a single surface Fresnel reflectance between air and Al_2O_3 (dashed line, calculated from the refractive index of Al_2O_3 thin films [27]).

Figure 9 compares the measured values of the 10 min etched structure with those of a random pyramidal texture typical for use in Si solar cells [15] and a polished Si sample [28]. In this context, it becomes clear that also b-Si structures with thicker Al_2O_3 coatings are suitable antireflection or light trapping structures, especially for broadband applications.

Considering the reflectance in figure 10 at wavelengths up to 2000 nm, for which Si is transparent, there is a reversal in the effect of the Al_2O_3 coatings. Up to 1100 nm wavelength, the reflectance is lower for thinner layer thicknesses, whereas for wavelengths above 1100 nm, the reflectance is
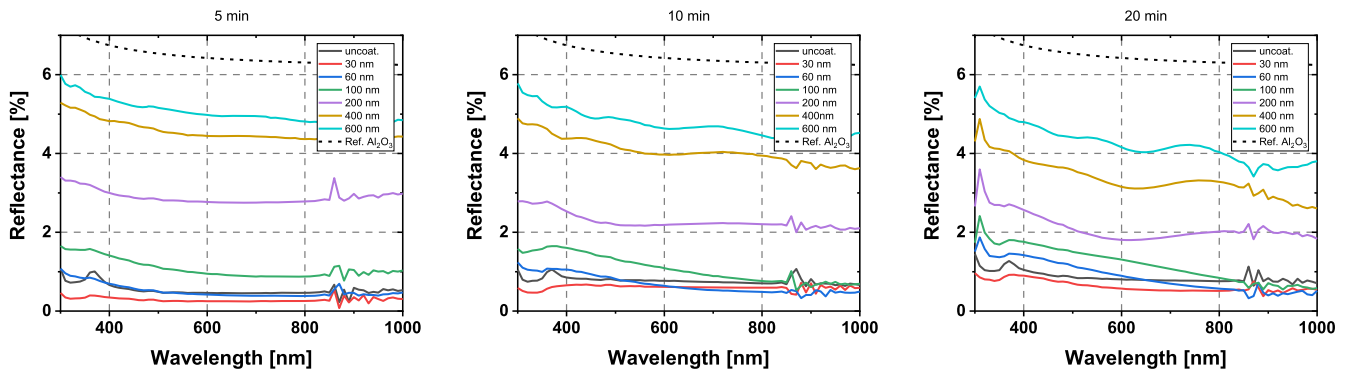
Figure 8. Reflectance of different b-Si samples coated with Al_2O_3 at varying layer thickness.
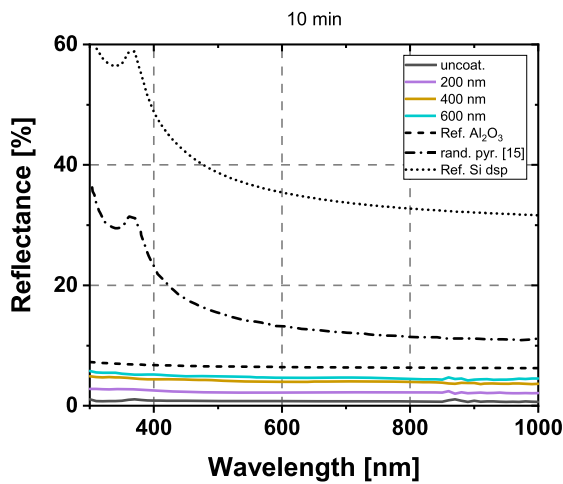

Figure 9. Comparison of Al_2O_3-coated b-Si structures with Fresnel reflectance air-Al_2O_3 (dashed), random pyramidal textures [15] (dashed–dotted) and polished Si (dotted).
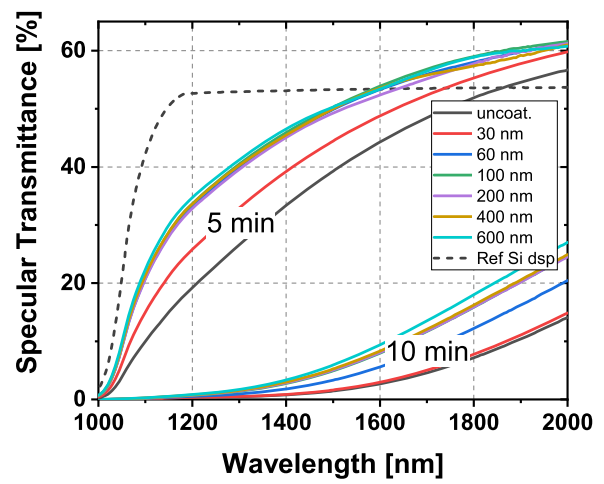

Figure 11. Specular transmittance in the SWIR spectral range for 5 and 10 min etched samples with varying Al_2O_3 layer thickness measured by Lambda 950 spectrometer.
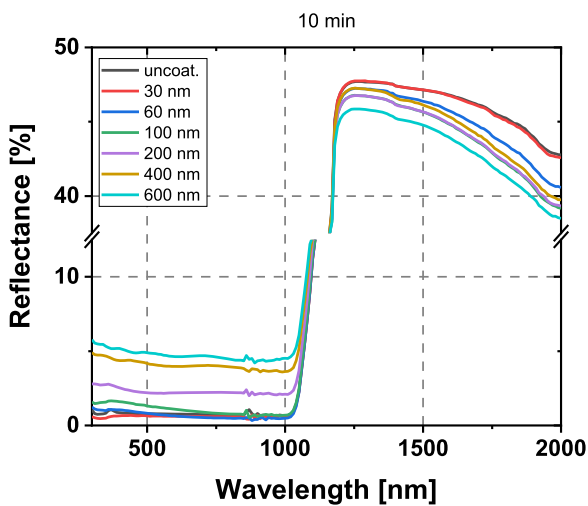

Figure 10. Reflectance of 10 min etched b-Si sample coated with Al_2O_3 at varying layer thickness.
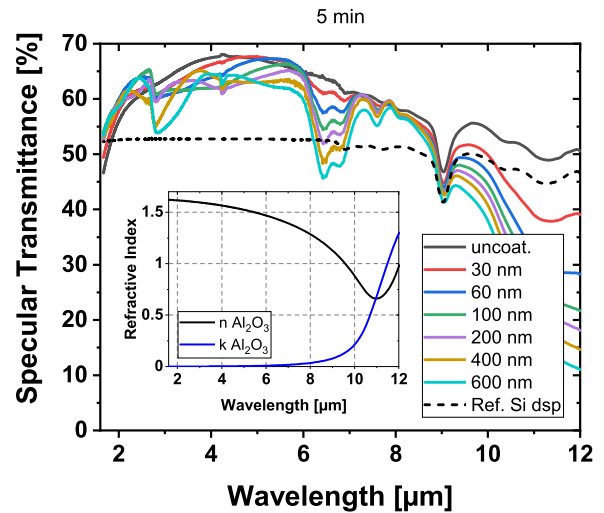

Figure 12. Specular transmittance of 5 min etched b-Si structure Al_2O_3-coated with varying thickness measured by FTIR. Inside is shown the refractive index of Al_2O_3.

lower for thicker Al_2O_3 coatings. We can assume that this effect is directly related to the transition of Si from an opaque to a transparent medium. For the thicker coatings we suppose a lower contrast in the refractive index and a higher amount of planarization. These two aspects reduce scattering and

increase the amount of specular light at the coated b-Si surface instead. The scattering of light, however, is essential for the effect of light trapping. While light trapping reduces the reflectance for absorbing materials, it is the opposite for
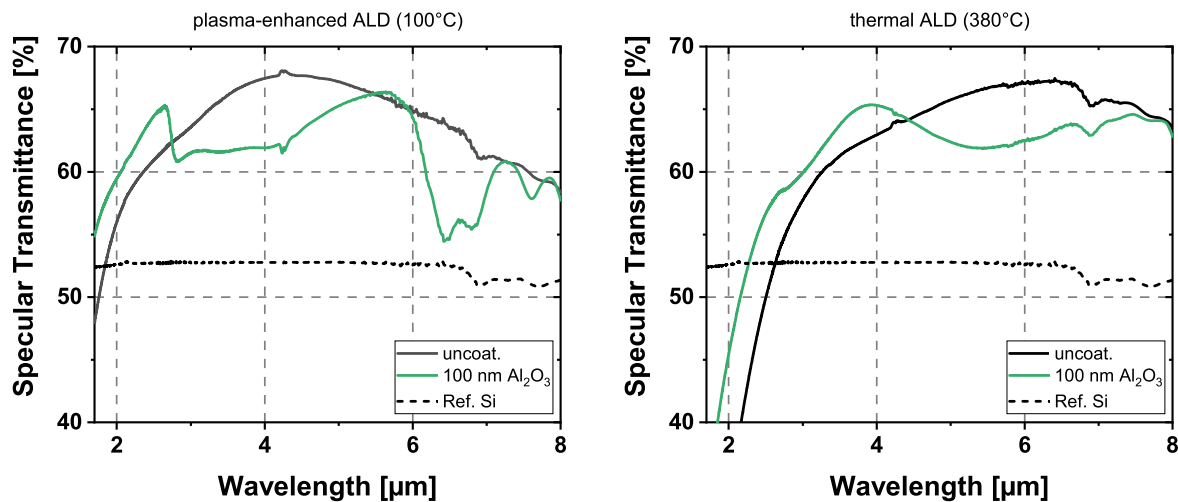
Figure 13. Comparison of the specular transmittance of b-Si structures with plasma-enhanced (left) and thermal (right) ALD coating.

transparent materials. Here, the reflection increases, as already discussed for the uncoated structures with different lateral dimensions in section 3.1 (see figure 2). Further research on this issue is beyond the scope of this paper. Yet, it is also in accordance with the measurements of the specular transmittance in the same spectral range displayed in figure 11.

Figure 11 shows the specular transmission of the coated b-Si structures measured with the Lambda 950 spectrometer. It is apparent that for an application in the SWIR, the lateral dimensions of the b-Si structures need to be smaller to prevent scattering and increase the specular transmittance.

Nevertheless, it becomes obvious that the specular transmission in the SWIR rises with higher Al_2O_3 layer thickness.

Further measurements in the FTIR spectrometer were carried out to study the influence of Al_2O_3 coatings on b-Si structures towards longer wavelengths. Figure 12 displays the specular transmission of the 5 min etched b-Si structures. Regarding its complex refractive index, Al_2O_3 coatings are only suitable for an application up to wavelengths of about 8 μm. For longer wavelengths, the extinction coefficient k of Al_2O_3 strongly increases [27], which makes a further application not very reasonable. With the larger amount of coated material due to the larger surface area of the b-Si structures, the absorption is even higher compared to coatings of the same thickness on polished surfaces.

Besides the element-specific absorption effect of Al_2O_3 for wavelengths above 8 μm, further absorption dips were observed for shorter wavelengths. The absorption dip at 2.8 μm wavelength (3570 cm^{-1}) is typical for PEALD and well described by Shestaeva *et al* [29]. It is based on OH stretching vibrations and strongly dependent on the coating temperature. The lower the temperature, the more hydroxylation and formation of OH groups occur [29]. The exact position of the absorption peak indicates the strength of the binding of the OH groups. The weak slope of the absorption dip towards longer wavelengths is also in accordance with the literature [29, 30]. Verlaan *et al* [30] furthermore describe the double peak at 6.25 μm (1600 cm^{-1}) and 6.76 μm (1480

cm^{-1}) wavelength that originates from CO vibrations. Again, it is strongly related to the process temperature during deposition. Thereby, the CO concentration decreases with increasing temperature. In the context of our studies, we could not confirm the described effect of an annealing step at 400 °C. The expected effect of absorption reduction by annealing did not occur. A further absorption dip is located at a wavelength of 7.6 μm. It is less prominent and assigned to symmetric OCO stretching vibrations of carbonate groups bound to alumina [31, 32].

For a reduction of the high impact of absorption, we deposited a 100 nm thick Al_2O_3 coating with a thermal ALD process at 380 °C process temperature using H_2O as oxygen source on an uncoated b-Si structure. The structures were subsequently measured in the FTIR spectrometer. Figure 13 compares the obtained results to those of a PEALD-coated b-Si structure with the same layer thickness of 100 nm. Due to a slight modification in the etching process of the used b-Si structure, the transmission curves of the initial uncoated structures are spectrally slightly shifted. However, the previously observed absorption dips completely disappeared for the thermal ALD coated structures.

4. Conclusion

This paper presents a broad study on the optical reflectance and transmittance properties of black silicon nanostructures functionalised with Al_2O_3 coatings applied by an ALD process. For this purpose, three b-Si structures with differing morphologies were optically characterised. The coating thickness varies here in a range between 30 and 600 nm.

In previous studies, electrical passivation of b-Si structures was the decisive reason for conformal coatings with thin Al_2O_3 up to several tens of nanometer in thickness. The investigation of thicker coatings was therefore not required. Mechanical stability, on the other hand, has not yet been taken into account in previous publications. However, it is a crucial aspect for the transfer of b-Si structures into broad

application. It is critical, not only for applications where the component is directly exposed to laboratory or outdoor environments, but also for components which are enclosed and meet several assembly steps including handling and cleaning. The mechanical stability is to be improved by embedding the structures in the coating material Al$_2$O$_3$, which is already used in the context of black silicon. The authors anticipate mechanical improvement even for thin coatings with less than 100 nm thickness, as a results of the increasing rounding of the previously sharply edged structures. With an increase in coating thickness, a further increase in stability is assumed. Due to the conformal coating, the b-Si nanostructures with depths of 1.2–3.3 μm were already fully embedded at a coating thickness of 400–600 nm, which promises additional reinforcement. Yet, it is important to evaluate whether the gain in mechanical robustness can be justified from an optical point of view.

For the optical characterisation, it is necessary to distinguish between two basic functions of the b-Si structures depending on the absorbance of Si. Up to wavelengths of 1.1 μm around the bandgap of Si, b-Si structures are mainly used as light trapping structures with transmissive scattering properties to maximize absorption and therefore minimize reflection. While for thin Al$_2$O$_3$ coatings the reflectance remains in the same range as for uncoated structures or is even slightly enhanced, the reflectance thereafter increases with increasing layer thickness. With the advantages in electrical passivation and mechanical stability, thin Al$_2$O$_3$ coatings up to 60 nm can be principally recommended. For coatings up to 200 nm, reflectance values of less than 2% were measured partially. Hence, this slight increase in reflectance could be significantly outweighed by the gain in additional mechanical stability. Nonetheless, for every coating thickness investigated, the reflectance of the whole structure system remains well below the Fresnel reflectance value of a single polished air-Al$_2$O$_3$ interface. In particular, the broadband low reflectance over the range from 300 to 1000 nm wavelength should be emphasised. Due to this broadband capability, the overcoated structures could, for example, be considered as an alternative for the random pyramidal textures typically used in Si photovoltaics.

For longer wavelengths than 1.1 μm, the focus is instead on antireflection properties with high specular transmittance for use in infrared optics. For shorter wavelengths than 2 μm, the investigated structures show a large amount of scattering, which makes them unsuitable for AR purposes in this spectral range. The deposition of an Al$_2$O$_3$ coating can increase the specular transmittance in this case due to the lower difference in refractive index. As demonstrated in this paper, it is feasible to find a suitable nanostructuring with an overcoated Al$_2$O$_3$ coating for an AR effect in the infraed spectral range up to 8 μm wavelength. For this, the selection of a suitable etching process with the appropriate process parameters as well as the consideration of the optical effect of the Al$_2$O$_3$ coating is important. A strong increase in the absorbance of Al$_2$O$_3$ prevents a reasonable application towards wavelengths longer than 8 μm. Depending on the applied ALD process and the process temperature, absorption dips occur also at shorter wavelengths.

This indicates hydroxylation of the Al$_2$O$_3$ coatings. To reduce these absorption effects, a thermal ALD process is recommended. When using a plasma-enhanced ALD process, a higher process temperature should be selected.

The aim of the investigations was to gain an understanding of the optical properties using ALD-coated nanostructures in order to find suitable compromises between optical enhancement and mechanical stability. The obtained findings provide a basis for future investigations on the mechanical stability of such coated nanostructures. Depending on potential applications, other coating materials can also be considered for investigation. Knowing that mechanical stability is a fundamental problem of black light-trapping and absorber structures, this paper aims to provide an impulse for further systematic research on nanostructures mechanically stabilised by ALD coatings.

Data availability statement

The data that support the findings of this study are available upon reasonable request from the authors.

ORCID iDs

David Schmelz https://orcid.org/0000-0002-5181-9919
Adriana Szeghalmi https://orcid.org/0000-0003-2055-2825
Uwe D Zeitner https://orcid.org/0000-0002-3980-6971

References

[1] Savin H, Repo P, Von Gastrow G, Ortega P, Calle E, Garín M and Alcubilla R 2015 Black silicon solar cells with interdigitated back-contacts achieve 22.1% efficiency *Nat. Nanotechnol.* **10** 624–8

[2] Liu X, Coxon P R, Peters M, Hoex B, Cole J M and Fray D J 2014 Black silicon: fabrication methods, properties and solar energy applications *Energy Environ. Sci.* **7** 3223–63

[3] Yuan H C, Yost V E, Page M R, Stradins P, Meier D L and Branz H M 2009 Efficient black silicon solar cell with a density-graded nanoporous surface: optical properties, performance limitations, and design rules *Appl. Phys. Lett.* **95** 123501

[4] Oh J, Yuan H C and Branz H M 2012 An 18.2%-efficient black-silicon solar cell achieved through control of carrier recombination in nanostructures *Nat. Nanotechnol.* **7** 743–8

[5] Steglich M, Lehr D, Ratzsch S, Käsebier T, Schrempel F, Kley E B and Tünnermann A 2014 An ultra-black silicon absorber *Laser Photon. Rev.* **8** L13–7

[6] Kimeu F, Albin S, Song K and Santiago K C 2021 ALD-passivated silicon nanowires for broadband absorption applications *AIP Adv.* **11** 065101

[7] Matsui Y and Adachi S 2013 Optical properties of 'black silicon' formed by catalytic etching of Au/Si(100) wafers *J. Appl. Phys.* **113** 173502

[8] Steglich M, Käsebier T, Schrempel F, Kley E B and Tünnermann A 2015 Self-organized, effective medium Black Silicon for infrared antireflection *Infrared Phys. Technol.* **69** 218–21

[9] Zhao Y, Anderson N C, Zhu K, Aguiar J A, Seabold J A, Lagemaat J V D and Oh J 2015 Oxidatively stable nanoporous silicon photocathodes with enhanced onset voltage for photoelectrochemical proton reduction *Nano Lett.* **15** 2517–25

[10] Zhang Z, Wang Y, Hansen P A S, Du K, Gustavsen K R, Liu G and Wang K 2019 Black silicon with order-disordered structures for enhanced light trapping and photothermic conversion *Nano Energy* **65** 103992

[11] Schmelz D, Steglich M, Dietrich K, Käsebier T and Zeitner U D 2019 Black-silicon-structured back-illuminated Ge-on-Si photodiode arrays *Integrated Optics: Design, Devices, Systems, and Applications V* 11031 (SPIE) pp 33–9

[12] Garin M, Heinonen J, Werner L, Pasanen T P, Vähänissi V, Haarahiltunen A and Savin H 2020 Black-silicon ultraviolet photodiodes achieve external quantum efficiency above 130% *Phys. Rev. Lett.* **125** 117702

[13] Juntunen M A, Heinonen J, Vähänissi V, Repo P, Valluru D and Savin H 2016 Near-unity quantum efficiency of broadband black silicon photodiodes with an induced junction *Nat. Photon.* **10** 777–81

[14] Wu S *et al* 2021 High-performance back-illuminated Ge 0.92 Sn 0.08/Ge multiple-quantum-well photodetector on Si platform for SWIR detection *IEEE J. Sel. Top. Quantum Electron.* **28** 1–9

[15] Manzoor S, Filipič M, Onno A, Topič M and Holman Z C 2020 Visualizing light trapping within textured silicon solar cells *J. Appl. Phys.* **127** 063104

[16] Von Gastrow G, Alcubilla R, Ortega P, Yli-Koski M, Conesa-Boj S, Morral I A F and Savin H 2015 Analysis of the atomic layer deposited Al_2O_3 field-effect passivation in black silicon *Sol. Energy Mater. Sol. Cells* **142** 29–33

[17] Hoex B, Gielis J J H, Van de Sanden M C M and Kessels W M M 2008 On the c-Si surface passivation mechanism by the negative-charge-dielectric Al_2O_3 *J. Appl. Phys.* **104** 113703

[18] Otto M, Kroll M, Käsebier T, Salzer R, Tünnermann A and Wehrspohn R B 2012 Extremely low surface recombination velocities in black silicon passivated by atomic layer deposition *Appl. Phys. Lett.* **100** 191603

[19] Plakhotnyuk M M, Gaudig M, Davidsen R S, Lindhard J M, Hirsch J, Lausch D and Hansen O 2017 Low surface damage dry etched black silicon *J. Appl. Phys.* **122** 143101

[20] Otto M 2015 Effective passivation of black silicon surfaces by conformal thermal ALD deposited Al_2O_3 layers *Doctoral Dissertation* Halle (Saale), Universitäts-und Landesbibliothek Sachsen-Anhalt, Diss.

[21] Singh A K, Adstedt K, Brown B, Singh P M and Graham S 2018 Development of ALD coatings for harsh environment applications *ACS Appl. Mater. Interfaces* **11** 7498–509

[22] Boryło P, Lukaszkowicz K, Szindler M, Kubacki J, Balin K, Basiaga M and Szewczenko J 2016 Structure and properties of Al_2O_3 thin films deposited by ALD process *Vacuum* **131** 319–26

[23] Dussart R, Mellhaoui X, Tillocher T, Lefaucheux P, Volatier M, Socquet-Clerc C and Ranson P 2005 Silicon columnar microstructures induced by an $SF6/O_2$ plasma *J. Phys. D: Appl. Phys.* **38** 3395

[24] Steglich M, Käsebier T, Zilk M, Pertsch T, Kley E B and Tünnermann A 2014 The structural and optical properties of black silicon by inductively coupled plasma reactive ion etching *J. Appl. Phys.* **116** 173503

[25] Yablonovitch E and Cody G D 1982 Intensity enhancement in textured optical sheets for solar cells *IEEE Trans. Electron Devices* **29** 300–5

[26] Campbell P and Green M A 1987 Light trapping properties of pyramidally textured surfaces *J. Appl. Phys.* **62** 243–9

[27] Kischkat J, Peters S, Gruska B, Semtsiv M, Chashnikova M, Klinkmüller M and Masselink W T 2012 Mid-infrared optical properties of thin films of aluminum oxide, titanium dioxide, silicon dioxide, aluminum nitride, and silicon nitride *Appl. Opt.* **51** 6789–98

[28] Green M A 2008 Self-consistent optical parameters of intrinsic silicon at 300 K including temperature coefficients *Sol. Energy Mater. Sol. Cells* **92** 1305–10

[29] Shestaeva S, Bingel A, Munzert P, Ghazaryan L, Patzig C, Tünnermann A and Szeghalmi A 2017 Mechanical, structural, and optical properties of PEALD metallic oxides for optical applications *Appl. Opt.* **56** C47–59

[30] Verlaan V, Van Den Elzen L R J G, Dingemans G, Van De Sanden M C M and Kessels W M M 2010 Composition and bonding structure of plasma-assisted ALD Al_2O_3 films *Phys. Status Solidi* C **7** 976–9

[31] Goldstein D N, McCormick J A and George S M 2008 Al_2O_3 atomic layer deposition with trimethylaluminum and ozone studied by *in situ* transmission FTIR spectroscopy and quadrupole mass spectrometry *J. Phys. Chem.* C **112** 19530–9

[32] Busca G and Lorenzelli V 1982 Infrared spectroscopic identification of species arising from reactive adsorption of carbon oxides on metal oxide surfaces *Mater. Chem.* **7** 89–126